Power-law decay of the fraction of the mixed eigenstates in kicked top model with mixed-type classical phase space

Qian Wang
CAMTP-Center for Applied Mathematics and Theoretical Physics, University of Maribor, Mladinska 3, SI-2000 Maribor, Slovenia, European Union
and Department of Physics, Zhejiang Normal University, Jinhua 321004, China

Marko Robnik
CAMTP-Center for Applied Mathematics and Theoretical Physics, University of Maribor, Mladinska 3, SI-2000 Maribor, Slovenia, European Union

(Received 9 August 2023; accepted 24 October 2023; published 17 November 2023)

The properties of mixed eigenstates in a generic quantum system with a classical counterpart that has mixed-type phase space, although important to understand several fundamental questions that arise in both theoretical and experimental studies, are still not clear. Here, following a recent work [Č. Lozej, D. Lukman, and M. Robnik, Phys. Rev. E **106**, 054203 (2022)], we perform an analysis of the features of mixed eigenstates in a time-dependent Hamiltonian system, the celebrated kicked top model. As a paradigmatic model for studying quantum chaos, the kicked top model is known to exhibit both classical and quantum chaos. The types of eigenstates are identified by means of the phase-space overlap index, which is defined as the overlap of the Husimi function with regular and chaotic regions in classical phase space. We show that the mixed eigenstates appear due to various tunneling precesses between different phase-space structures, while the regular and chaotic eigenstates are, respectively, associated with invariant tori and chaotic components in phase space. We examine how the probability distribution of the phase-space overlap index evolves with increasing system size for different kicking strengths. In particular, we find that the relative fraction of mixed states exhibits a power-law decay as the system size increases, indicating that only purely regular and chaotic eigenstates are left in the strict semiclassical limit. We thus provide further verification of the principle of uniform semiclassical condensation of Husimi functions and confirm the correctness of the Berry-Robnik picture.

DOI: 10.1103/PhysRevE.108.054217

I. INTRODUCTION

The pivotal role played by the quantum chaos in studying various important questions in numerous branches of physics has triggered a great deal of efforts to explore different aspects of quantum chaos [1–10]. However, a full understanding of the properties of the quantum systems associated with classical mixed-type systems is still lacking. Classically, the mixed-type systems exhibit both regular and chaotic motion and result in an intricate hierarchical structure in their phase space, with regular islands embedded in the chaotic sea [11]. This led Percival to conjecture that the eigenstates in the corresponding quantum systems should be of either the regular or the chaotic type [12]. With further elaboration made by Berry [13,14], this conjecture finally develops into the so-called principle of uniform semiclassical condensation (PUSC) of Wigner functions (or Husimi functions) [15]. For details, see recent review papers [16,17] and references therein.

According to the PUSC, the eigenstates in a generic quantum system are either condensed on the invariant tori in the regular islands, referred to as the regular states, or supported on the chaotic sea, known as the chaotic states, in the ultimate semiclassical limit where the classical action is much larger than the Planck constant. Consequently, the spectral statistics for the regular and chaotic states are separately described by the Poissonian statistics [18] and random matrix theory [19–21], while the whole spectrum is well captured by the Berry-Robnik (BR) picture [22]. The validity of the BR distribution to characterize the spectral statistics in generic quantum systems has been numerically verified by numerous works [23–32]. However, in the near semiclassical limit, it is natural to expect that there should be an intermediate regime in which many eigenstates will behave as mixed states due to various tunneling processes between different phase-space structures. Although the mixed eigenstates exhibit several important and interesting phenomena, such as chaos-assisted tunneling [33], which has potential applications in quantum simulation [34] and can be used to create highly entangled states [35], much of their properties remain unknown.

Very recently, using the Husimi function [36], the properties of the mixed states in the lemon billiards [37–41] have been explored [42]. It was found that the fraction of the mixed eigenstates shows a power-law decay as the semiclassical limit is approached. Although the PUSC and the BR distribution are valid for any systems that have mixed-type classical phase space, the answer to the question of how the fraction of the mixed eigenstates varies with approaching the semiclassical limit in time-periodic systems remains unknown. In the present work, we continue and extend previous study to provide a detailed investigation of the signatures of the mixed

states in a time-periodic system, i.e., the kicked top model [43], a paradigmatic model in the study of quantum chaos [3], which has been realized in a variety of experimental platforms, such as cold atoms [44], superconducting circuits [45], and nuclear magnetic resonance simulators [46]. As the kicked top model exhibits a transition from the regular regime to the chaotic one with increasing kicking strength [3,43], it therefore provides us with a model system to analyze the features of the mixed states in time-periodic systems.

Following the method used in Ref. [42], the mixed states are identified by the phase-space overlap index defined through the Husimi functions of the eigenstates. We show that the probability distribution of the phase-space overlap index has a double-peak shape and bears a remarkable change as the semiclassical limit is approached (namely, by increasing the system size). More insights about the properties of the mixed states are gained from the dependence of their proportion on the system size. We demonstrate that the proportion of mixed states which belong to a certain interval of the phase-space overlap index follows a power-law decay with increasing system size. This confirms the disappearance of the relative fraction of the mixed states in the semiclassical limit, as unveiled in lemon billiards and in consistence with the PUSC. It further verifies the correctness of the Berry-Robnik picture for describing the spectral statistics in generic quantum systems.

The structure of the article is the following. In Sec. II, we introduce the kicked top model and analyze the integrability-chaos transition for classical and quantum cases by means of the largest Lyapunov exponent and Kolmogorov-Sinai entropy, as well as the spectral statistics, respectively. In addition, the definition and calculation of the Husimi function for an individual eigenstate are also discussed in this section. Then, in Sec. III, we perform an explicit analysis of the probability distribution of the phase-space overlap index, showing how it evolves with increasing system size. In this section, we further examine the dependence of the proportion of mixed states on the system size. We finally conclude in Sec. IV with several remarks.

II. KICKED TOP MODEL

The model we study is the kicked top model, which is a time-dependent system with the Hamiltonian given by (setting $\hbar = 1$) [43]

$$H = \alpha J_x + \frac{\gamma}{2j} J_z^2 \sum_{n=-\infty}^{+\infty} \delta(t-n), \tag{1}$$

where J_ν, with $\nu = x$, y, and z, are the angular momentum operators of the total spin j system. α denotes the angle of the precession around the x axis, and γ is the strength of the kicking with a period that we have set to unity. It is worth pointing out that the dependence of both quantum and classical dynamics of the model on the value of α has been investigated in our previous work [47]. Here, we have numerically verified that our main results, namely, the statistics of the phase-space overlap index and the power-law decay of the fraction of the mixed eigenstates as a function of the system size, are independent of the specific value of α. We thus set $\alpha = 11\pi/19$ throughout this work.

The dynamical evolution under the above Hamiltonian is governed by the Floquet operator

$$F = e^{-i\frac{\gamma}{2j}J_z^2} e^{-i\alpha J_x}. \tag{2}$$

One can easily find that the Hamiltonian (1) conserves the total spin j. Hence, the Hilbert space of the system has the dimension $\mathcal{D}_\mathcal{H} = 2j+1$. In our numerical calculation, the basis for the Hilbert space is the Dicke states, $\{|j,m\rangle\}_{m=-j}^{m=+j}$, satisfying $J_z|j,m\rangle = m|j,m\rangle$ and $\mathbf{J}^2|j,m\rangle = j(j+1)|j,m\rangle$, with $\mathbf{J}^2 = J_x^2 + J_y^2 + J_z^2$. Then, the elements of the Floquet operator are

$$\langle j,m|F|j,m'\rangle = \exp\left(-i\frac{\gamma}{2j}m^2\right)\mathcal{W}_{mm'}, \tag{3}$$

where $\mathcal{W}_{mm'}$ is the Winger D function [48] and can be calculated as

$$\begin{aligned}\mathcal{W}_{mm'} &= \langle j,m|e^{-i\alpha J_x}|j,m'\rangle \\ &= \sum_{k_x=-j}^{k_x=+j} e^{-i\alpha k_x}\langle j,m|j,k_x\rangle\langle j,k_x|j,m'\rangle,\end{aligned} \tag{4}$$

with $|j,k_x\rangle$ representing the eigenstates of J_x, so that $J_x|j,k_x\rangle = k_x|j,k_x\rangle$.

The time evolution of the angular momentum is given by the map $J_\nu(n+1) = F^\dagger J_\nu(n) F$, which can be explicitly written as [43,49,50]

$$\begin{aligned}J_x(n+1) &= \frac{1}{2}\{J_x(n) + i\Theta_n(\alpha)\}\exp\left[i\frac{\gamma}{2j}\Xi_n(\alpha)\right] + \text{H.c.},\\ J_y(n+1) &= \frac{1}{2i}\{J_x(n) + i\Theta_n(\alpha)\}\exp\left[i\frac{\gamma}{2j}\Xi_n(\alpha)\right] + \text{H.c.},\\ J_z(n+1) &= J_y(n)\sin\alpha + J_z(n)\cos\alpha,\end{aligned} \tag{5}$$

where $\Theta_n(\alpha) = J_y(n)\cos\alpha - J_z(n)\sin\alpha$ and $\Xi_n(\alpha) = 2[J_y(n)\sin\alpha + J_z(n)\cos\alpha] + 1$. A detailed derivation of the above equations can also be found in Appendix of Ref. [51].

A. Classical kicked top model

The classical counterpart of the kicked top model is obtained by taking the classical limit $j \to \infty$, which means that one can define an effective Planck constant as $\hbar_{\text{eff}} = 1/j$. To obtain the classical equations of motion of the kicked top model, we first introduce the normalized vector $\mathbf{X} = \langle\mathbf{J}\rangle/j$, which becomes a classical vector when $j \to \infty$. Then, as the expectation value of the products of the evolved angular momentum operators in Eq. (5) can be factorized as $\langle J_\mu J_\nu\rangle = \langle J_\mu\rangle\langle J_\nu\rangle$ in the classical limit, it is straightforward to show that the classical map for the classical vector $\mathbf{X}$ takes the form [50,52]

$$\begin{bmatrix}X_{n+1}\\ Y_{n+1}\\ Z_{n+1}\end{bmatrix} = \begin{bmatrix}\cos\Omega_n & -\cos\alpha\sin\Omega_n & \sin\alpha\sin\Omega_n\\ \sin\Omega_n & \cos\alpha\cos\Omega_n & -\sin\alpha\cos\Omega_n\\ 0 & \sin\alpha & \cos\alpha\end{bmatrix}\begin{bmatrix}X_n\\ Y_n\\ Z_n\end{bmatrix}, \tag{6}$$

where $\Omega_n = \gamma(Y_n\sin\alpha + Z_n\cos\alpha)$. The normalization of $\mathbf{X}$ allows us to parametrize it as $\mathbf{X} = (\cos\phi\sin\theta, \sin\phi\sin\theta, \cos\theta)$,

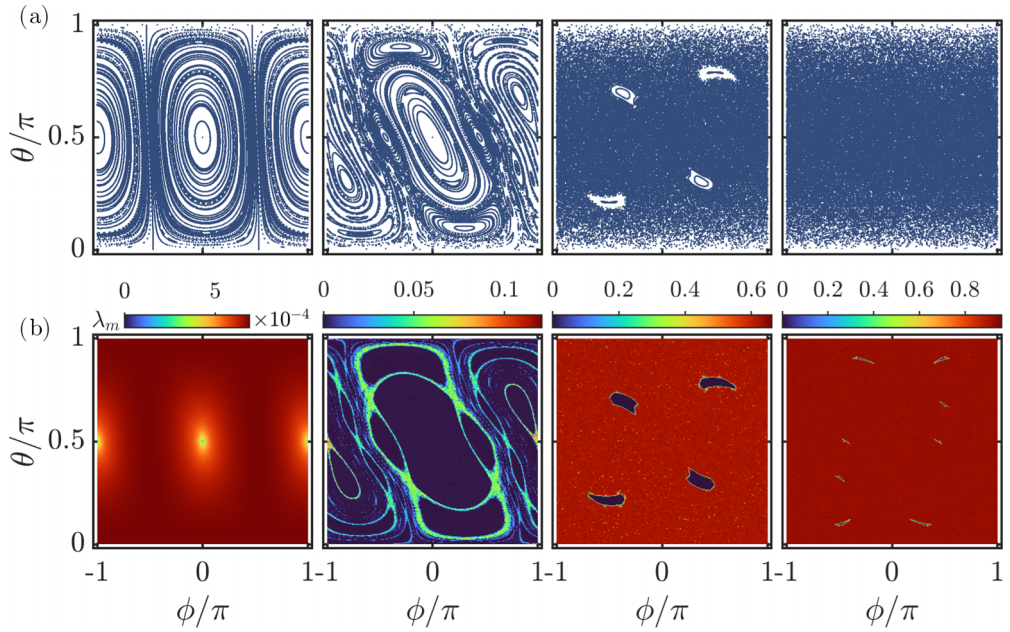

FIG. 1. (a) Classical phase-space portraits with 225 random initial conditions for (from left to right) $\gamma = 0.2$, 2, 4, and 6. Each initial condition has been evolved for 400 kicks. (b) The largest Lyapunov exponent λ_m of the classical kicked top model for the same values of γ as in panel (a). The largest Lyapunov exponent has been calculated on a grid of 300×300 initial conditions; each has a duration of 1×10^4 kicks. Other parameter: $\alpha = 11\pi/19$.

with θ and ϕ being the azimuthal and polar angles, respectively. Hence, the classical phase space can be described by the variables $\phi = \arctan(Y/X)$ and $\theta = \arccos(Z)$.

It is known that the classical map in Eq. (6) undergoes a transition from integrability to chaos with increasing the kicking strength γ. This is demonstrated in Fig. 1(a), where we plot the Poincaré section of the classical top model for different γ values. It can be clearly seen that the classical phase space is dominated by regular orbits for small γ and turns into the mixed dynamics with regular islands embedded in the chaotic sea as γ is increased. The regular islands disappear for even larger γ and the phase space is fully covered by the chaotic sea, as shown in the right-most column of Fig. 1(a).

To quantitatively capture the chaotic transition illustrated in Fig. 1(a), we consider the largest Lyapunov exponent, which describes the rate of the deviation between two initially nearby close orbits and can be calculated as [11,52]

$$\lambda_m = \lim_{t\to\infty} \frac{1}{t} \sum_{n=1}^{t} \ln d_n, \tag{7}$$

where $d_n = [(\delta X_n)^2 + (\delta Y_n)^2 + (\delta Z_n)^2]^{1/2}$ is the phase-space distance between two initially nearby points after n kicks. Here, $\delta\mathbf{X}$ is determined by the tangent map [52], and $\delta\mathbf{X}_{n+1} = [\partial\mathbf{X}_{n+1}/\partial\mathbf{X}_n]\delta\mathbf{X}_n$, with the initial condition $\delta\mathbf{X}_0$. Moreover, we renormalize d_n at each step n in our calculation. As the largest Lyapunov exponent quantifies how two infinitesimal orbits separate with time, it therefore acts as a measure of the level of chaos. For the regular regions in the phase space, we have $\lambda_m = 0$, while $\lambda_m > 0$ for the chaotic component.

Figure 1(b) plots the largest Lyapunov exponent for the same values of γ as in Fig. 1(a). A remarkable resemblance between Figs. 1(a) and 1(b) can be obviously observed. Specifically, the very tiny λ_m at small γ is in agreement with the regular dynamics, as seen in the first column of Fig. 1. For the mixed phase space, one can see that the $\lambda_m = 0$ regions are clearly corresponding to the regular regions in the phase space, while the chaotic regions are marked by $\lambda_m > 0$, as demonstrated in the second and third columns of Fig. 1. The globally chaotic dynamics at $\gamma = 6$ results in the larger values and an almost uniform distribution of the largest Lyapunov exponent in the phase space (see the last column of Fig. 1). In particular, the largest Lyapunov exponent can help us identify the invisible regular islands in the Poincaré section.

Further characterizations of the integrability-chaos transition in the classical kicked top model are revealed by the Kolmogorov-Sinai (KS) entropy, which is, generally speaking, related to the rate of change of the coarse-grained Gibbs entropy with time [53] and for the kicked top model is calculated as [11,54]

$$S_{\mathrm{KS}} = \frac{1}{4\pi} \int \lambda_m d\mathcal{A}, \tag{8}$$

where $d\mathcal{A} = \sin\theta d\theta d\phi$ is the phase-space area element [55]. Figure 2(a) shows how the KS entropy S_{KS} varies with increasing γ. The value of S_{KS} remains 0 for $\gamma \leqslant 2$ and begins to grow at $\gamma > 2$. This means that the model undergoes a chaotic transition around $\gamma = 2$ and the degree of chaoticity is enhanced with increasing γ, in accord with the phase-space features shown in Fig. 1(a). Here, we would like to point out that the plateau in the behavior of S_{KS} around $\gamma \approx 6$ is due to the existence of tiny regular regions in the classical phase space [see the last panel in Fig. 1(b)].

B. Quantum chaos in kicked top model

The onset of chaos in the classical kicked top model gets reflected in its quantum counterpart, resulting in the quantum

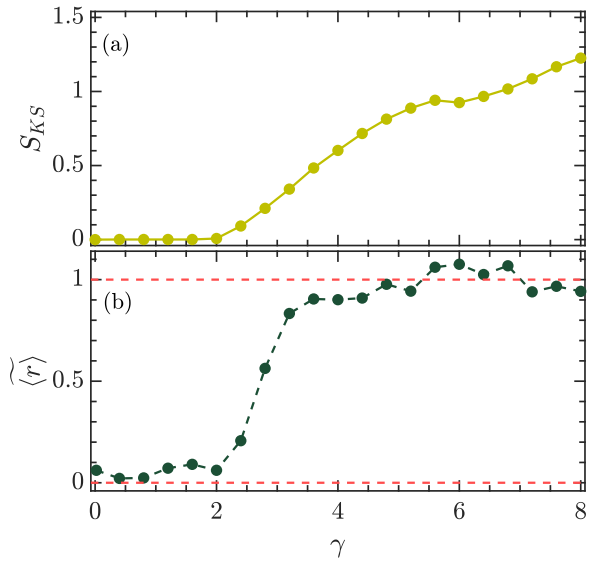

FIG. 2. (a) Kolmogorov-Sinai (KS) entropy, $S_{\rm KS}$, as a function of kicking strength γ. $S_{\rm KS}$ is obtained by averaging over 90 000 initial points in the phase space, each evolved for 1×10^4 kicks. (b) Variation of the rescaled average level spacing ratio with γ for $j = 2500$. The upper and lower red dashed lines denote $\widetilde{\langle r \rangle} = 1$ and 0, respectively. Other parameter: $\alpha = 11\pi/19$.

chaos. There are many different ways to diagnose the presence of quantum chaos [56–62]. Among them, the statistics of the spacings s between consecutive energy levels is the most commonly used probe. The distribution of s in the chaotic systems is well described by the Wigner surmise [19,20], whereas the regular systems are generically characterized by the Poisson distribution [18,63]. Here, instead of analyzing the level spacing distribution, we focus on the spacing ratio for three successive levels, first introduced in Ref. [64]. The big advantage to consider the level spacing ratios rather than the level spacings themselves is that it avoids the intricate unfolding procedure. As a consequence, it becomes the most popular chaos indicator in various studies [9,51,65–73], in particular. for many-body quantum systems.

For the time-dependent Hamiltonian, such as our studied model, the level spacing ratios are defined as

$$r_n = \min\left(\frac{s_n}{s_{n-1}}, \frac{s_{n-1}}{s_n}\right), \tag{9}$$

where $s_n = \nu_n - \nu_{n-1}$, with ν_n being the nth quasienergy (eigenphase) of the Floquet operator in Eq. (2). Clearly, r is defined in the range $0 \leqslant r \leqslant 1$. The distribution $P(r)$ of r for both integrable and chaotic systems has been analytically derived [65,74], from which one can find that the mean level spacing ratio, $\langle r \rangle = \int_0^1 rP(r)dr$, behaves as an efficient detector of quantum chaos. For integrable systems, one has $\langle r \rangle_{\rm RG} = 2\ln 2 - 1 \approx 0.386$ [65], while $\langle r \rangle_{\rm COE} \approx 0.527$ [66,67] for the fully chaotic systems belonging to the circular orthogonal ensemble (COE), which describes the systems with antisymmetry. It is known that the Floquet operator of the kicked top model satisfies [43,75]

$$\mathcal{T} F \mathcal{T}^{-1} = F, \tag{10}$$

where $\mathcal{T} = e^{-\alpha J_x} e^{i\pi J_y} \mathcal{T}_0$, with $\mathcal{T}_0$ being the conventional time-reversal operator, so that $\mathcal{T}_0 \mathbf{J} \mathcal{T}_0^{-1} = -\mathbf{J}$. One can therefore expect that the statistics of the eigenphases of F must be given by COE [43,66]. As a result, the mean level spacing ratio of the kicked top model should equal to $\langle r \rangle_{\rm COE}$ for $\gamma \gtrsim 5$.

A more convenient quantity that is used to detect the crossover from integrability to quantum chaos is the rescaled mean level spacing ratio [51,76], defined as

$$\widetilde{\langle r \rangle} = \frac{|\langle r \rangle - \langle r \rangle_{\rm RG}|}{\langle r \rangle_{\rm COE} - \langle r \rangle_{\rm RG}}. \tag{11}$$

It varies in the interval $\widetilde{\langle r \rangle} \in [0, 1]$. When $\widetilde{\langle r \rangle} = 0$, it indicates the regular dynamics in the system. On the contrary, the fully chaotic dynamics in the system leads to $\widetilde{\langle r \rangle} = 1$. In Fig. 2(b), we display how $\widetilde{\langle r \rangle}$ evolves as a function of γ. We can see that the transition of $\widetilde{\langle r \rangle}$ from a value close to 0 to a value around 1 confirms the onset of chaos as γ is increased. Moreover, the agreement between the onset of chaos in $S_{\rm KS}$ and $\widetilde{\langle r \rangle}$ at $\gamma \approx 2$ further corroborates a good quantum-classical correspondence.

C. Husimi function

Our aim is to explore the properties of the eigenstates in a quantum system with mixed phase space in the classical limit. It is therefore required to identify the various types of the eigenstates. As in previous works [17,77–80], we use the Husimi function [36] to characterize the signatures of the eigenstates in classical phase space.

The Husimi function can unveil various aspects of the eigenstates exhibited in the phase space, in particular, their localization properties [42,51,81–85]. To define the Husimi function for the kicked top model, we first introduce the generalized SU(2) spin-coherent states, defined as a rotation of the Dicke state $|j, j\rangle$, which can be explicitly written as [86–88]

$$\begin{aligned} |\phi, \theta\rangle &= e^{i\theta(J_x \sin\phi - J_y \cos\phi)} |j, j\rangle \\ &= \sum_{m=-j}^{+j} \frac{\xi^{j-m}}{(1+|\xi|^2)^j} \sqrt{\frac{(2j)!}{(j+m)!(j-m)!}} |j, m\rangle, \end{aligned} \tag{12}$$

where $\xi = \tan(\theta/2) e^{i\phi}$ with $\phi \in [-\pi, \pi)$ and $\theta \in [0, \pi]$. The overcompleteness of the coherent states results in the following closure relation:

$$\mathbb{I} = \frac{2j+1}{4\pi} \int |\phi, \theta\rangle\langle\phi, \theta| \sin\theta d\theta d\phi. \tag{13}$$

Then the Husimi function for the nth eignestate, $|\nu_n\rangle$, of F in Eq. (2) is given by

$$Q_n(\phi, \theta) = |\langle\theta, \phi|\nu_n\rangle|^2, \tag{14}$$

with the normalization condition

$$\frac{2j+1}{4\pi} \int Q_n(\phi, \theta) \sin\theta d\theta d\phi = 1. \tag{15}$$

The principle of uniform semiclassical condensation of the Wigner and Husimi functions predicts that the Husimi functions will condense either on the classically invariant torus or the chaotic regions in the semiclassical limit. However, before the semiclassical limit is reached in practice, one expects that there should exist mixed eigenstates with associated Husimi

functions occupying both regular and chaotic regions. In the following section, we identify these mixed states by means of the phase-space overlap index and discuss how their relative fraction varies as the semiclassical limit is approached. We demonstrate that it decays as a power law.

III. PHASE-SPACE OVERLAP INDEX

Armed with the Husimi function, let us discuss how to identify the types of the eigenstates using the approach that has been performed in Refs. [42,77,79]. We divide the classical phase space (ϕ, θ) into a grid with cells of equal area. Each cell is marked by its center point with the index (i, j). We then define a discrete quantity C_{ij}, which takes the value $+1$ if the grid point (i, j) resides in the chaotic regions and -1 otherwise. Accordingly, the Husimi function of the nth eigenstate is discretized on the grid and normalized as $[(2j+1)\pi/(2N)]\sum_{i,j}\sin\theta_j Q_n(\phi_i,\theta_j) = 1$, with N being the number of grid points. In our calculation, we construct and generate the chaotic region through a single sufficiently long and dense chaotic orbit. To this end, we randomly choose an initial condition in the chaotic region and evolve it for 10^6 kicks. Consequently, all regular regions and possibly smaller chaotic regions are included in the complement. As these smaller chaotic regions are so tiny, they can be neglected and considered as a part of regular region.

To elucidate whether the nth eigenstate is the regular or the chaotic eigenstate, we define an overlap index:

$$M_n = \frac{(2j+1)\pi}{2N}\sum_{i,j}\sin\theta_j Q_n(\phi_i,\theta_j)C_{ij}. \tag{16}$$

In the ultimate semiclassical limit, one can expect that M should take the value either -1 or $+1$, corresponding to the regular or chaotic eigenstates, respectively. However, since the semiclassical limit is not yet reached in practice, M actually varies between -1 and $+1$. Hence, it is natural to ask what is the distribution of M and how it changes as the semiclassical limit is approached.

Previously, the joint distribution of M and the phase-space localization measures have been analyzed in the billiard systems and it was found that the distribution of M turns into a double-peak distribution when approaching the semiclassical limit [42]. In addition, approaching the semiclassical limit also led to a power-law decay of the proportion of the mixed states with intermediate values of M. In the following of this section, we address the abovementioned questions in the kicked top model and provide further evidence of the power-law decay exhibited by the fraction of the mixed states in the semiclassical limit. In this work, the grid that we used has 200×400 points, so that $N = 8 \times 10^4$. Surely, at the given j we must have a sufficiently large number of grid points to warrant a correct resolution of the mixed states. We have checked that our main conclusions still hold for further increasing N. Obviously, the larger the system size j is, the larger the total number of grid points that is required.

Let us first consider the probability distribution of M, which is defined as

$$P(M \in \Lambda_n) = \frac{1}{\mathcal{D}_\mathcal{H}}\sum_{M_k\in\Lambda_n}\delta_{M,M_k}, \tag{17}$$

where $\Lambda_n = [M_n, M_n + dM]$ and $\mathcal{D}_\mathcal{H} = 2j+1$ is the Hilbert space dimension. $P(M)$ quantifies the probability of finding M in an infinitesimal interval $M \in \Lambda_n$.

In Fig. 3(a), we show the histogram of $P(M)$ for the kicked top model with $j \in [150, 154]$, $\gamma = 2.6$, and $\alpha = 11\pi/19$. Clearly, $P(M)$ behaves as a continuous distribution over the range $M \in [-1, 1]$ and has two expected sharp clusters around $M = -1$ and $M = +1$, corresponding to regular and chaotic eigenstates, respectively. The existence of the intermediate values of M indicates that apart from the regular and chaotic eigenstates, there also exist many mixed eigenstates. To see this, we plot the Husimi function for several eigenstates with different M values in Figs. 3(c) and 3(d). Comparing to the classical Poincaré section in Fig. 3(b), one can see that the regular eigenstate with $M = -1$ is entirely localized in the regular island [Fig. 3(c)], while the chaotic eigenstate with $M = +1$ exhibits a quite uniform distribution over the chaotic sea, as illustrated in Fig. 3(f). For the eigenstates with intermediate values of M, we see the tunneling between different regular island chains [cf. Fig. 3(d)], as well as between the regular region and chaotic component, as demonstrated in Fig. 3(e).

Further properties of $P(M)$ are revealed in Fig. 4, where we plot $P(M)$ for several system size ensembles with different kicking strengths. Based on these results we make the following observations.

(i) As the semiclassical limit is approached with increasing j, the larger the value of j is, the more the eigenstates move towards the regular or chaotic clusters, regardless of the γ value.

(ii) The fluctuations among the intermediate values of M are suppressed as the system size j is increased.

(iii) Increasing γ leads to an enhancement in the level of chaos, resulting in $P(M)$ exhibiting a high peak around $M = 1$ and tiny fluctuations for $-1 < M < 1$.

The evolution of $P(M)$ observed in Fig. 4 allows us to conclude that the relative fraction of the mixed eigenstates decreases with increasing system size. To verify this statement and to quantitatively characterize the behaviors observed in Fig. 4, we investigate how the proportion of the mixed states varies as a function of the system size j. To this end, we choose an interval ΔM in the range $-1 < M < 1$ and consider the relative fraction of the mixed states belonging to ΔM, defined as

$$f_{\rm mix} = \frac{\mathcal{N}_{\rm mix}^{\Delta M}}{\mathcal{D}_\mathcal{H}}, \tag{18}$$

where $\mathcal{N}_{\rm mix}^{\Delta M}$ is the total number of the mixed states in ΔM and $\mathcal{D}_\mathcal{H} = 2j+1$ denotes the Hilbert space dimension.

In Fig. 5, we plot how $f_{\rm mix}$ evolves as a function of the ensemble-averaged system size $\langle j\rangle$ for different γ and ΔM values. Overall, we see that irrespective of the values of γ and ΔM, the decay of $f_{\rm mix}$ with increasing $\langle j\rangle$ is well described by the power law of the form $f_{\rm mix} \sim \langle j\rangle^{-\zeta}$. However, the decay rate ζ depends on both γ and ΔM. Besides, when we compare the y-axis scale in Fig. 5(a) with Fig. 5(b), we observe that $f_{\rm mix}$ undergoes a drastic decrease as γ is increased, consistent with the results in Fig. 4. Clearly, with γ increasing the chaos increases and thus the number of mixed states decreases as well. Furthermore, due to the larger fluctuations in $P(M)$ for

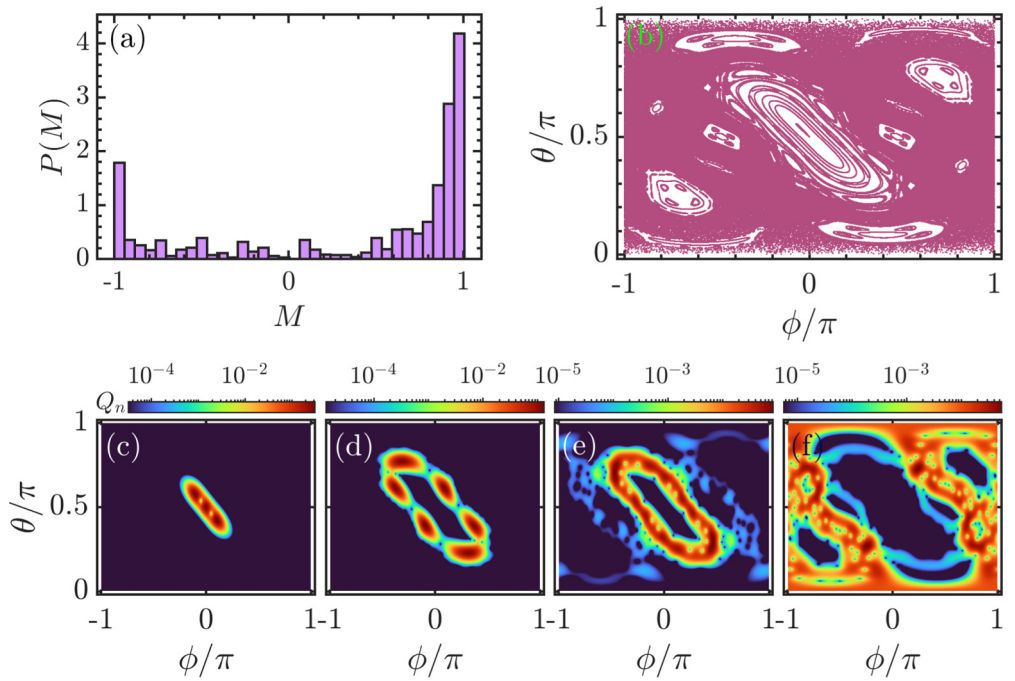

FIG. 3. (a) Histogram of the probability distribution $P(M)$ for the kicked top model with $\gamma = 2.6$. The histogram is obtained for the eigenstates of the system with sizes $j \in [150, 154]$, increasing in steps of 1. (b) Poincaré section of the kicked top model for $\gamma = 2.6$. (c)–(f) Husimi functions for the eigenstates $n = 5$, $M_n = -1$ (c); $n = 36$, $M_n = -0.5161$ (d); $n = 10$, $M_n = 0.3075$ (e); and $n = 264$, $M_n = 0.9744$ (f), with $j = 150$ and $\gamma = 2.6$. Other parameter: $\alpha = 11\pi/19$.

small ΔM, the degree of agreement between the numerical data and the power-law decay decreases with decreasing ΔM. But, as the fluctuations in $P(M)$ reduce with increasing system size, one can expect a substantial improvement in the quality of the power-law fitting for larger system sizes. Moreover, a careful numerical check has confirmed that the power-law decay of f_{mix} with respect to the system size is independent of the size of ΔM and the position of the interval. However, we can expect that different choices of intervals and ΔM should affect the decay exponent ζ.

Let us discuss the dependence of the decay exponent ζ on the different choices of intervals with $\Delta M = 0.4$.

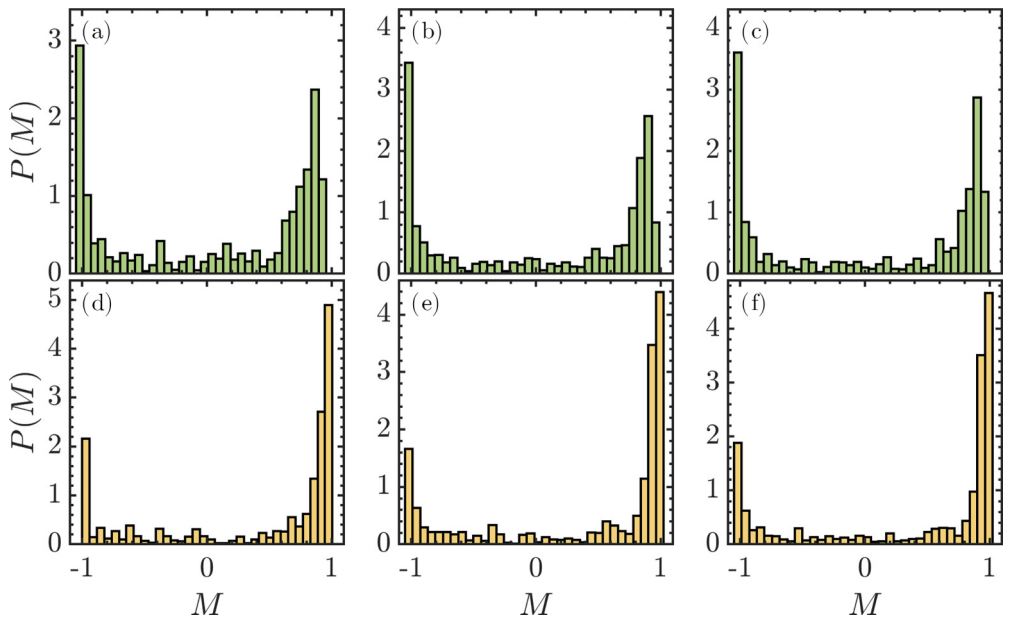

FIG. 4. (a)–(c) Histograms of $P(M)$ for different ensembles of the system size: (a) $j \in [200, 204]$, (b) $j \in [300, 304]$, and (c) $j \in [400, 404]$. The kicking strength is $\gamma = 2.3$. (d)–(f) Histograms of $P(M)$ for the same system size ensembles as in panels (a)–(c) with $\gamma = 2.6$. Other parameter: $\alpha = 11\pi/19$. The system size j in each ensemble is increased in steps of 1.

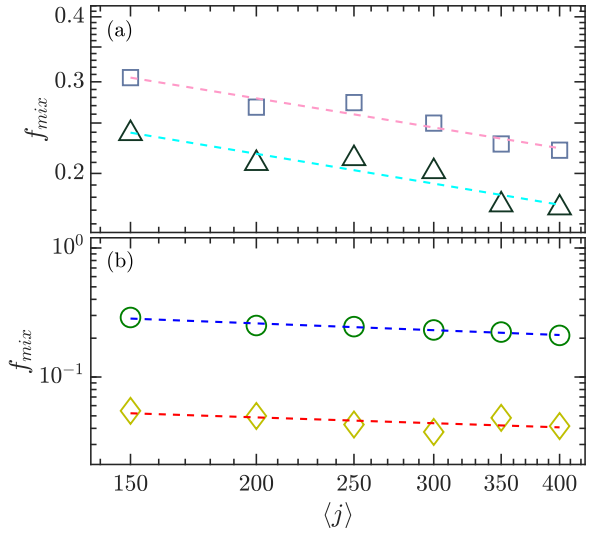

FIG. 5. (a) Proportion of mixed states f_{mix} as a function of ensemble-averaged system size $\langle j \rangle$ for the eigenstates with $M \in [-0.8, 0.6]$ (squares) and $M \in [-0.5, 0.6]$ (triangles). The pink and cyan dot-dashed lines denote the fitting curves of the power law $f_{\text{mix}} \propto \langle j \rangle^{-\zeta}$, with $\zeta = 0.3184$ and $\zeta = 0.3253$, respectively. The kicking strength for this case is $\gamma = 2.3$. (b) f_{mix} as a function of $\langle j \rangle$ for $M \in [-0.8, 0.7]$ (circles) and $M \in [-0.2, 0.2]$ (diamonds) with $\gamma = 2.6$. The blue and red dashed lines are the power-law fitting curves, $f_{\text{mix}} \propto \langle j \rangle^{-\zeta}$, with $\zeta = 0.2986$ and $\zeta = 0.2561$. Other parameter: $\alpha = 11\pi/19$. The system size ensemble for each $\langle j \rangle$ is given by $j \in [\langle j \rangle - 5, \langle j \rangle + 5]$, increasing in steps of 1.

The results for two different kicking strengths are plotted in Fig. 6. A prominent feature observed in the behavior of ζ is its larger fluctuations, regardless of the kicking strength. This stems from the fact that fluctuations in $P(M)$ vary with the choice of intervals, as seen in Fig. 4. However, the enhancement of the degree of chaoticity with increasing γ gives rise to a remarkable decrease of the fluctuations in the behavior of ζ. Moreover, as $P(M)$ becomes more smooth as

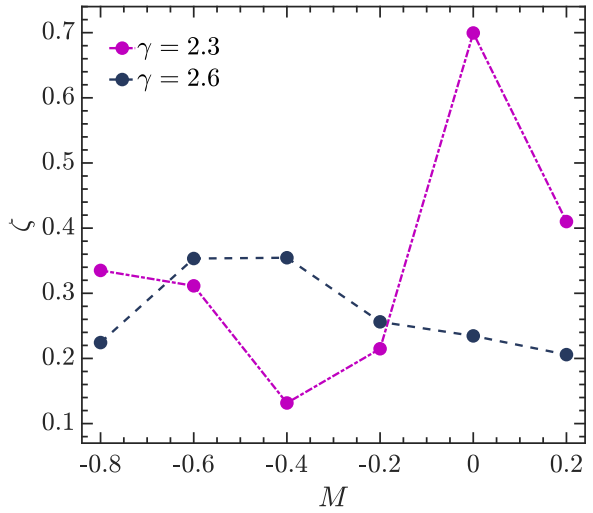

FIG. 6. Power-law decay exponent ζ for $M \in [M + \Delta M]$, with $\Delta M = 0.4$. The curves correspond to different kicking strengths. Other parameter: $\alpha = 11\pi/19$.

the system size increases, one can expect that the fluctuations in ζ will be suppressed for larger system sizes. Note that the behavior of ζ studied here is distinguished from the one revealed in billiard systems, where ζ exhibits a rather smooth dependence on the value of M for fixed ΔM [42].

The power-law decay of the proportion of mixed states has also been observed in billiards, but the decay exponent is different from our considered model [42]. A general understanding of the underlying mechanism of such a difference suggests the need for further exploration. Nevertheless, the similar decay behavior exhibited by the two different systems leads us to conjecture that the power-law decay is a universal property of the relative fraction of the mixed states, independent of any specific system. A theoretical investigation of the decay behavior of the relative fraction of mixed states would be a very interesting topic for our future work. Here, we would like to point out that a detailed analysis of the tunneling [89–92] and flooding [93,94] effects in mixed quantum systems is necessary to obtain a better understanding of the properties of the mixed eigenstates in the semiclassical limit.

IV. CONCLUSIONS

In summary, we have performed a detailed analysis of the properties of the mixed states in the kicked top model. Being a prototype model for studying quantum chaos, the kicked top model is known for exhibiting a transition to chaos for both classical and quantum cases [3] which is unveiled by various chaos indicators and shows a good quantum-classical correspondence between them. For chosen values of kicking strength, the classical phase space of the kicked top model exhibits a complex structure with several regular islands coexisting with a dominating uniform chaotic component. This indicates that the eigenstates of the analogous quantum counterpart should also have different types of behavior.

To identify the types of the eigenstates, we employ the Husimi function to define the phase-space overlap index M, which measures the degree of overlap of the Husimi function with chaotic and regular regions in the classical phase space. The definition of M implies that it will ideally take the value $+1$ for fully chaotic eigenstates, while for purely regular eigenstates it equals -1. However, we have shown that it varies between -1 and $+1$ in the near semiclassical limit with $-1 < M < 1$ corresponding to the mixed states characterized by various tunneling processes among different phase-space structures.

Further features of the mixed states are revealed by the probability distribution of M. We have demonstrated that the distribution of M has two peaks at $M = \pm 1$, which become more sharp with increasing system size (i.e., approaching the semiclassical limit), agreeing with the prediction of the principle of uniform semiclassical condensation (PUSC) of Wigner functions (or Husimi functions) [16,17]. A quantitative description of the signatures exhibited by the probability distribution of M is provided by the proportion of the mixed states with associated M belonging to a given interval. We have shown that the dependence of the proportion of the mixed states on the system size is well captured by the power-law decay whose exponent varies for different choices of the interval and kicking strengths. Therefore, one can

expect that the relative fraction of the mixed states will disappear in the far semiclassical limit, confirming the statement of the PUSC.

The same power-law decay of the proportion of mixed states observed in billiards [42] allows us to conjecture that the proportion of mixed states in other mixed-type systems should also decay as a power law in the semiclassical limit. A natural extension of the present work is to systematically study the properties of mixed states in quantum systems with a well-defined classical limit, such as the Dicke model [81,83,95–99], the coupled top model [100,101], and the three-site Bose-Hubbard model [102–104]. Another open topic that deserves investigation is to establish a general theoretical understanding of the power-law decay demonstrated by mixed states. Finally, it is worth pointing out that confirmation of the PUSC in the kicked top model provides further evidence of the correctness of the Berry-Robnik picture in the analysis of spectral statistics of generic quantum systems.

ACKNOWLEDGMENTS

This work was supported by the Slovenian Research and Innovation Agency (ARIS) under Grants No. J1-4387 and No. P1-0306. Q.W. acknowledges support from the National Science Foundation of China (NSFC) under Grant No. 11805165 and the Zhejiang Provincial Nature Science Foundation under Grant No. LY20A050001.

[1] F. M. Izrailev, Phys. Rep. **196**, 299 (1990).
[2] H.-J. Stöckmann, *Quantum Chaos: An Introduction* (Cambridge University, Cambridge, England, 1999).
[3] F. Haake, *Quantum Signatures of Chaos*, Physics and Astronomy Online Library (Springer, Berlin, 2001).
[4] D. Ullmo, Rep. Prog. Phys. **71**, 026001 (2008).
[5] J. M. G. Gómez, K. Kar, V. Kota, R. Molina, A. Relaño, and J. Retamosa, Phys. Rep. **499**, 103 (2011).
[6] F. Borgonovi, F. Izrailev, L. Santos, and V. Zelevinsky, Phys. Rep. **626**, 1 (2016).
[7] L. D'Alessio, Y. Kafri, A. Polkovnikov, and M. Rigol, Adv. Phys. **65**, 239 (2016).
[8] V. Jahnke, Adv. High Energy Phys. **2019**, 1 (2019).
[9] L. Sá, P. Ribeiro, and T. Prosen, Phys. Rev. X **10**, 021019 (2020).
[10] A. Dymarsky and A. Gorsky, Phys. Rev. B **102**, 085137 (2020).
[11] A. Lichtenberg and M. Lieberman, *Regular and Chaotic Dynamics*, Applied Mathematical Sciences (Springer, New York, 2013).
[12] I. C. Percival, J. Phys. B: At. Mol. Phys. **6**, L229 (1973).
[13] M. V. Berry, J. Phys. A: Math. Gen. **10**, 2083 (1977).
[14] M. V. Berry and J. M. Ziman, Philos. Trans. R. Soc. London., Ser. A **287**, 237 (1977).
[15] M. Robnik, Nonlinear Phenom. Complex Syst. **1**, 1 (1998).
[16] M. Robnik, Recent advances in quantum chaos of generic systems, in *Encyclopedia of Complexity and Systems Science*, edited by R. A. Meyers (Springer, Berlin, 2019), pp. 1–17.
[17] M. Robnik, Nonlinear Phenom. Complex Syst. **23**, 172 (2020).
[18] M. V. Berry, M. Tabor, and J. M. Ziman, Proc. R. Soc. A **356**, 375 (1977).
[19] O. Bohigas, M. J. Giannoni, and C. Schmit, Phys. Rev. Lett. **52**, 1 (1984).
[20] E. P. Wigner, Characteristic vectors of bordered matrices with infinite dimensions, in *The Collected Works of Eugene Paul Wigner: Part A: The Scientific Papers*, edited by A. S. Wightman (Springer, Berlin, 1993), pp. 524–540.
[21] M. Mehta, *Random Matrices* (Elsevier, Amsterdam, 2004).
[22] M. V. Berry and M. Robnik, J. Phys. A: Math. Gen. **17**, 2413 (1984).
[23] T. Prosen and M. Robnik, J. Phys. A: Math. Gen. **26**, 2371 (1993).
[24] T. Prosen and M. Robnik, J. Phys. A: Math. Gen. **27**, 8059 (1994).
[25] T. Prosen and M. Robnik, J. Phys. A: Math. Gen. **27**, L459 (1994).
[26] B. Li and M. Robnik, J. Phys. A: Math. Gen. **27**, 5509 (1994).
[27] T. Prosen, J. Phys. A: Math. Gen. **28**, L349 (1995).
[28] B. Li and M. Robnik, J. Phys. A: Math. Gen. **28**, 4843 (1995).
[29] T. Prosen, J. Phys. A: Math. Gen. **31**, 7023 (1998).
[30] T. Prosen and M. Robnik, J. Phys. A: Math. Gen. **32**, 1863 (1999).
[31] G. Veble, M. Robnik, and J. Liu, J. Phys. A: Math. Gen. **32**, 6423 (1999).
[32] T. Manos and M. Robnik, Phys. Rev. E **87**, 062905 (2013).
[33] S. Tomsovic and D. Ullmo, Phys. Rev. E **50**, 145 (1994).
[34] M. Martinez, O. Giraud, D. Ullmo, J. Billy, D. Guéry-Odelin, B. Georgeot, and G. Lemarié, Phys. Rev. Lett. **126**, 174102 (2021).
[35] G. Vanhaele, A. Bäcker, R. Ketzmerick, and P. Schlagheck, Phys. Rev. A **106**, L011301 (2022).
[36] K. Husimi, Proc. Phys. Math. Soc. Jpn. **22**, 264 (1940).
[37] E. J. Heller and S. Tomsovic, Phys. Today **46**, 38 (1993).
[38] H. Makino, T. Harayama, and Y. Aizawa, Phys. Rev. E **63**, 056203 (2001).
[39] Č. Lozej, D. Lukman, and M. Robnik, Phys. Rev. E **103**, 012204 (2021).
[40] Č. Lozej, D. Lukman, and M. Robnik, Physics **3**, 888 (2021).
[41] Č. Lozej, D. Lukman, and M. Robnik, Nonlinear Phenom. Complex Syst. **24**, 1 (2021).
[42] Č. Lozej, D. Lukman, and M. Robnik, Phys. Rev. E **106**, 054203 (2022).
[43] F. Haake, M. Kuś, and R. Scharf, Z. Phys. B **65**, 381 (1987).
[44] S. Chaudhury, A. Smith, B. E. Anderson, S. Ghose, and P. S. Jessen, Nature (London) **461**, 768 (2009).
[45] C. Neill, P. Roushan, M. Fang, Y. Chen, M. Kolodrubetz, Z. Chen, A. Megrant, R. Barends, B. Campbell, B. Chiaro, A. Dunsworth, E. Jeffrey, J. Kelly, J. Mutus, P. J. J. O'Malley, C. Quintana, D. Sank, A. Vainsencher, J. Wenner, T. C. White *et al.*, Nat. Phys. **12**, 1037 (2016).
[46] V. R. Krithika, V. S. Anjusha, U. T. Bhosale, and T. S. Mahesh, Phys. Rev. E **99**, 032219 (2019).
[47] Q. Wang and M. Robnik, Entropy **23**, 1347 (2021).
[48] M. Rose, *Elementary Theory of Angular Momentum*, Dover Books on Physics and Chemistry (Dover, New York, 1995).

[49] R. F. Fox and T. C. Elston, Phys. Rev. E **50**, 2553 (1994).
[50] M. H. Muñoz-Arias, P. M. Poggi, and I. H. Deutsch, Phys. Rev. E **103**, 052212 (2021).
[51] Q. Wang and M. Robnik, Phys. Rev. E **107**, 054213 (2023).
[52] A. Piga, M. Lewenstein, and J. Q. Quach, Phys. Rev. E **99**, 032213 (2019).
[53] A. N. Kolmogorov, Dokl. Akad. Nauk SSSR **124**, 754 (1959).
[54] Y. B. Pesin, Russ. Math. Surv. **32**, 55 (1977).
[55] G. M. D'Ariano, L. R. Evangelista, and M. Saraceno, Phys. Rev. A **45**, 3646 (1992).
[56] T. Guhr, A. Müller-Groeling, and H. A. Weidenmüller, Phys. Rep. **299**, 189 (1998).
[57] J. Emerson, Y. S. Weinstein, S. Lloyd, and D. G. Cory, Phys. Rev. Lett. **89**, 284102 (2002).
[58] E. Lantagne-Hurtubise, S. Plugge, O. Can, and M. Franz, Phys. Rev. Res. **2**, 013254 (2020).
[59] M. Zonnios, J. Levinsen, M. M. Parish, F. A. Pollock, and K. Modi, Phys. Rev. Lett. **128**, 150601 (2022).
[60] S. Wimberger, Aspects of quantum chaos, in *Nonlinear Dynamics and Quantum Chaos: An Introduction* (Springer, Cham, 2022), pp. 153–253.
[61] I. García-Mata, R. A. Jalabert, and D. A. Wisniacki, Scholarpedia **18**, 55237 (2023).
[62] K. Hashimoto, K. Murata, N. Tanahashi, and R. Watanabe, arXiv:2305.16669.
[63] M. Robnik and G. Veble, J. Phys. A: Math. Gen. **31**, 4669 (1998).
[64] V. Oganesyan and D. A. Huse, Phys. Rev. B **75**, 155111 (2007).
[65] Y. Y. Atas, E. Bogomolny, O. Giraud, and G. Roux, Phys. Rev. Lett. **110**, 084101 (2013).
[66] L. D'Alessio and M. Rigol, Phys. Rev. X **4**, 041048 (2014).
[67] O. Giraud, N. Macé, E. Vernier, and F. Alet, Phys. Rev. X **12**, 011006 (2022).
[68] A. M. García-García, B. Loureiro, A. Romero-Bermúdez, and M. Tezuka, Phys. Rev. Lett. **120**, 241603 (2018).
[69] P. Sierant and J. Zakrzewski, Phys. Rev. B **99**, 104205 (2019).
[70] A. L. Corps and A. Relaño, Phys. Rev. E **101**, 022222 (2020).
[71] S. Moudgalya, A. Prem, D. A. Huse, and A. Chan, Phys. Rev. Res. **3**, 023176 (2021).
[72] Q. Wang, Entropy **24**, 1415 (2022).
[73] J. Mateos, F. Sols, and C. Creffield, arXiv:2306.09785.
[74] Y. Y. Atas, E. Bogomolny, O. Giraud, P. Vivo, and E. Vivo, J. Phys. A: Math. Theor. **46**, 355204 (2013).
[75] M. Kus, J. Mostowski, and F. Haake, J. Phys. A: Math. Gen. **21**, L1073 (1988).
[76] P. Łydżba and T. Sowiński, Phys. Rev. A **106**, 013301 (2022).
[77] B. Batistić and M. Robnik, J. Phys. A: Math. Theor. **46**, 315102 (2013).
[78] B. Batistić and M. Robnik, Phys. Rev. E **88**, 052913 (2013).
[79] M. Robnik, Eur. Phys. J.: Spec. Top. **225**, 959 (2016).
[80] Č. Lozej and M. Robnik, Phys. Rev. E **98**, 022220 (2018).
[81] Q. Wang and M. Robnik, Phys. Rev. E **102**, 032212 (2020).
[82] Q. Wang and F. Pérez-Bernal, Phys. Rev. E **104**, 034119 (2021).
[83] D. Villaseñor, S. Pilatowsky-Cameo, M. A. Bastarrachea-Magnani, S. Lerma-Hernández, and J. G. Hirsch, Phys. Rev. E **103**, 052214 (2021).
[84] S. Pilatowsky-Cameo, D. Villaseñor, M. A. Bastarrachea-Magnani, S. Lerma-Hernández, L. F. Santos, and J. G. Hirsch, Quantum **6**, 644 (2022).
[85] S. Pilatowsky-Cameo, D. Villaseñor, M. A. Bastarrachea-Magnani, S. Lerma-Hernández, and J. G. Hirsch, Phys. Rev. E **105**, 064209 (2022).
[86] J. M. Radcliffe, J. Phys. A: Gen. Phys. **4**, 313 (1971).
[87] A. M. Perelomov, Sov. Phys. Usp. **20**, 703 (1977).
[88] W.-M. Zhang, D. H. Feng, and R. Gilmore, Rev. Mod. Phys. **62**, 867 (1990).
[89] S. Tomsovic, Phys. Scr. **T90**, 162 (2001).
[90] V. A. Podolskiy and E. E. Narimanov, Phys. Rev. Lett. **91**, 263601 (2003).
[91] A. Bäcker, R. Ketzmerick, S. Löck, M. Robnik, G. Vidmar, R. Höhmann, U. Kuhl, and H.-J. Stöckmann, Phys. Rev. Lett. **100**, 174103 (2008).
[92] A. Bäcker, R. Ketzmerick, S. Löck, and L. Schilling, Phys. Rev. Lett. **100**, 104101 (2008).
[93] A. Bäcker, R. Ketzmerick, and A. G. Monastra, Phys. Rev. Lett. **94**, 054102 (2005).
[94] A. Bäcker, R. Ketzmerick, and A. G. Monastra, Phys. Rev. E **75**, 066204 (2007).
[95] C. Emary and T. Brandes, Phys. Rev. E **67**, 066203 (2003).
[96] M. A. Bastarrachea-Magnani, B. López-del Carpio, J. Chávez-Carlos, S. Lerma-Hernández, and J. G. Hirsch, Phys. Rev. E **93**, 022215 (2016).
[97] S. Lerma-Hernández, D. Villaseñor, M. A. Bastarrachea-Magnani, E. J. Torres-Herrera, L. F. Santos, and J. G. Hirsch, Phys. Rev. E **100**, 012218 (2019).
[98] R. J. Lewis-Swan, A. Safavi-Naini, J. J. Bollinger, and A. M. Rey, Nat. Commun. **10**, 1581 (2019).
[99] Á. L. Corps, R. A. Molina, and A. Relaño, J. Phys. A: Math. Theor. **55**, 084001 (2022).
[100] D. Mondal, S. Sinha, and S. Sinha, Phys. Rev. E **102**, 020101(R) (2020).
[101] D. Mondal, S. Sinha, and S. Sinha, Phys. Rev. E **105**, 014130 (2022).
[102] M. Rautenberg and M. Gärttner, Phys. Rev. A **101**, 053604 (2020).
[103] K. Wittmann W., E. R. Castro, A. Foerster, and L. F. Santos, Phys. Rev. E **105**, 034204 (2022).
[104] G. Nakerst and M. Haque, Phys. Rev. E **107**, 024210 (2023).